Nanosensors Based on Viologen Functionalized Silver Nanoparticles: Few Molecules Surface. Enhanced Raman Spectroscopy Detection of Polycyclic Aromatic Hydrocarbons in Interparticle...

ARTICLE *in* ANALYTICAL CHEMISTRY · MARCH 2009

Impact Factor: 5.64 · DOI: 10.1021/ac8021746 · Source: PubMed

Anal. Chem. **2009,** *81,* 1418–1425

Nanosensors Based on Viologen Functionalized Silver Nanoparticles: Few Molecules Surface-Enhanced Raman Spectroscopy Detection of Polycyclic Aromatic Hydrocarbons in Interparticle Hot Spots

Luca Guerrini,* José V. Garcia-Ramos, Concepción Domingo, and Santiago Sanchez-Cortes

Instituto de Estructura de la Materia, CSIC, Serrano, 121, 28006-Madrid, Spain

The functionalization of silver nanoparticles (Ag NPs) by viologen dications (VGDs) is reported in this work as well as their applications in the surface-enhanced Raman scattering (SERS) detection of polycyclic aromatic hydrocarbons (PAHs). VGDs are able to form intermolecular cavities at interparticle junctions (SERS hot spots) where the analyte can be allocated. This leads to a giant intensification of the Raman emission of the target molecule. This effect was applied in the detection of PAHs, one of the most widespread and dangerous group of pollutants existing in the atmosphere and waters. A comparison between sensing-systems based on different VGDs (lucigenin, diquat, and paraquat) was done for the detection of two PAHs (pyrene and benzo[*c*]phenanthrene). The functionalization with lucigenin (LG) provided the most powerful and stable VGD-NPs sensor, which allowed the SERS detection of pyrene (PYR) down to 10^{-9} M in the macro setup and in the zeptomole range for spectra obtained by single NPs aggregates (micro setup). Besides, SERS spectra afforded important structural information about the interaction mechanism of VGD and PAHs, revealing the formation of a CT complex between the VGD and PYR and changes in the host conformation. The position of the *ν*(Ag−Cl) band and the plasmon resonance contribution assigned to Ag dimers were also used as spectral markers to monitor the host−guest interaction.

Surface-enhanced Raman spectroscopy (SERS) is an extremely highly sensitive technique based mainly on the giant electromagnetic (EM) enhancement induced by nanostructured noble metal surfaces and associated with their localized plasmon resonance (LPR).[1,2] SERS represented a great advance in the field of the Raman spectroscopy due to the large increase of the Raman cross section, as a result of the intensification of both the incident and the emitted radiations in the scattering process.[1] This makes SERS a useful analytical tool widely applied, for instance, in single molecule detection (SMD)[3,4] or few molecules detection (FMD).[5,6] Moreover, in the last years there has been a general acceptance that SERS spectroscopy has evolved to the stage where it can be used as a quantitative analytical technique.[7]

However, SMD or FMD were mainly applied in the detection of molecules having a large Raman cross section and under resonant conditions. Besides, the near field character of plasmon localization requires a close proximity of the analyte to the surface, which implies a high affinity to bind the metal. Unfortunately, many persistent organic pollutants (POPs) display a much lower Raman cross section than the dyes due to their poor affinity toward the metal surface, thus making difficult the application of SERS to their detection.

The affinity toward the metal surface can be increased with the functionalization of the metal surface by host molecules or cavitands. In previous works we have employed this strategy to detect polycyclic aromatic hydrocarbons (PAHs).[8−12] The host has to fulfill several requirements: (a) display strong affinity to both the metal and the analyte, (b) the adoption of a good self-assembly organization on the metal−liquid interface with the presence of cavities with an appropriate size, (c) high selectivity, (d) no self-association or formation of multilayers, and (e) absence or low band overlapping with the Raman features of the target molecule.

On the other hand, the low cross section of POPs can be further increased by inducing their adsorption at or near the interparticle gaps, where the main part of the electromagnetic field

* To whom correspondence should be addressed. E-mail: lucaguerrini@cfmac.csic.es.

(1) Moskovits, M. *Rev. Mod. Phys.* **1985**, *57*, 783–826.
(2) Aroca, R. *Surface-Enhanced Vibrational Spectroscopy*; John Wiley & Sons: Chichester, U.K., 2006.
(3) Kneipp, K.; Kneipp, H.; Itzkan, I.; Dasari, R. R.; Feld, M. S. *Chem. Rev.* **1999**, *99*, 2957–2975.
(4) Constantino, C. J. L.; Lemma, T.; Antunes, P. A.; Aroca, R. *Anal. Chem.* **2001**, *73*, 3674–3678.
(5) Bjerneld, E. J.; Johansson, P.; Kall, M. *Single Mol.* **2000**, *1*, 239–248.
(6) Xu, H. X.; Bjerneld, E. J.; Kall, M.; Borjesson, L. *Phys. Rev. Lett.* **1999**, *83*, 4357–4360.
(7) Bell, S. E. J.; Sirimuthu, N. M. S. *Chem. Soc. Rev.* **2008**, *37*, 1012–1024.
(8) Leyton, P.; Sanchez-Cortes, S.; Campos-Vallette, M.; Domingo, C.; Garcia-Ramos, J. V.; Saitz, C. *Appl. Spectrosc.* **2005**, *59*, 1009–1015.
(9) Leyton, P.; Sanchez-Cortes, S.; Garcia-Ramos, J. V.; Domingo, C.; Campos-Vallette, M.; Saitz, C.; Clavijo, R. E. *J. Phys. Chem. B* **2004**, *108*, 17484–17490.
(10) Guerrini, L.; Garcia-Ramos, J. V.; Domingo, C.; Sanchez-Cortes, S. *Langmuir* **2006**, *22*, 10924–10926.
(11) Guerrini, L.; Garcia-Ramos, J. V.; Domingo, C.; Sanchez-Cortes, S. *Anal. Chem.* **2008**, *81*, 953−960.
(12) Guerrini, L.; Jurasekova, Z.; Domingo, C.; Perez-Mendez, M.; Leyton, P.; Campos-Vallette, M.; Garcia-Ramos, J. V.; Sanchez-Cortes, S. *Plasmonics* **2007**, *2*, 147–156.

10.1021/ac8021746 CCC: $40.75
Published on Web 01/21/2009

intensification occurs.[13−15] These highly sensitive junctions are commonly referred to as hot spots (HS). In recent works, the selectively enhanced formation of HS by using bifunctional linkers has been reported.[16,17] In general, the ideal host molecule is that acting both as HS inducer and as cavitand, i.e., creating intra or intermolecular cavities just inside the hot spot in order to maximize the SERS intensification of the analyte Raman emission.

For this purpose, in this work we have employed viologen dications (VGDs) in the functionalization of the metal surface. VGD species join together different properties of interest which make them a promising group of hosts for POPs detection. In fact, they are electron acceptors,[18,19] thus able to interact strongly with the metal surface and able to form CT complexes with electron donor species such as polycyclic aromatic hydrocarbons.[18] As a result, the functionalization of Ag nanoparticles (NPs) is a strategy which can be specifically employed to the detection of these important pollutants. The hosting capability of VGDs is due to the repulsion between the positive charges of these dications, which influences their self-organization on the surface generating the formation of intermolecular cavities. Furthermore, their bifunctional nature makes VGDs able to induce the formation of HS. The VGDs paraquat (PQ), diquat (DQ), and lucigenin (LG) were assayed in this work in order to accomplish a comparative study of their abilities in detecting PAHs.

Identification and quantification of PAHs in water solution is usually carried out by HPLC with UV−visible, fluorimetric, or amperometric detection or by means of GC/MS or GC/FID, and most of them include a preconcentration step. These steps are time-consuming and require a great deal of effort, thus making the analysis unsuitable for routine control analysis.

The preparation of VGD based nanosensors was made by using Ag NPs in suspension, since only in these systems a previous modification of the aggregation architecture is possible so that to enable the VGD-driven formation of the HS. Several molecular markers were employed to test the sensing ability of VGD-AgNPs systems: more specifically, SERS features of both VGDs and PAHs, the ν(Ag−Cl) band, and the plasmon resonance contribution assigned to Ag dimers.

EXPERIMENTAL SECTION

Materials. Lucigenin dinitrate was purchased from Aldrich with a purity of >97% w/w. Diquat dibromide monohydrate was purchased from Chem Service with a purity of >99% w/w. Paraquat dichloride was purchased from Aldrich with a purity of >98% w/w. 9-(Methylaminomethyl)-anthracene (MAMA) was purchased from Aldrich with a purity of >99% w/w. Aqueous stock solutions of the VGD were prepared in Milli-Q water. All the reagents employed were of analytical grade. Pyrene (PYR) and benzo[*c*]phenanthrene (BcP) were purchased from Aldrich with a purity of 99% w/w and 98% w/w, respectively, and used as received. Stock solutions of these compounds in acetone (99%) were prepared to a final concentration of 10^{-2} M.

Ag NPs were prepared by reduction of silver nitrate with citrate following the method of Lee and Meisel.[20] In previous works we have characterized the morphology of these NPs, as well as their aggregation and the effect of anions.[21−23]

SERS measurements on Ag colloid suspensions were performed first by adding an aliquot of aqueous chloride solution to a final concentration of 3×10^{-2} M, then by adding an aliquot of VGD solutions up to the desired concentration. Eventually, in the case of VGD/PYR complexes, appropriate aliquots of the PYR or BcP solution were added. The effect of the Cl^- is double: it induces the aggregation of Ag colloid and promotes the adsorption of the viologens via a strong ionic interaction. The SERS measurements were carried out both in macro and microconditions. Macro SERS spectra were registered using 1 cm optical path cuvettes. Micro-SERS measurements were carried out by immobilizing the colloidal NPs on a glass and using a 100× objective (Scheme S1, see the Supporting Information).

Instrumentation. FT-Raman and FT-SERS spectra were obtained with a Bruker RFS 100/S instrument by using the line at 1064 nm provided by a Nd:YAG laser and a Ge detector cooled by liquid nitrogen. The resolution was set to 4 cm^{-1}, and 180° geometry was employed. The output laser power was 50 mW. The solid samples were placed in a brass holder. Up to 1000 scans were accumulated.

The SERS spectra were measured with a Renishaw Raman microscope system RM2000 equipped with argon laser at 514.5 nm and a diode laser at 785 nm, a Leica microscope, and an electrically refrigerated CCD camera. The laser power in the sample was 2.0 mW. The spectral resolution was set at 2 cm^{-1}. The microspectra shown here were obtained by using a 100× objective.

Samples for UV−visible absorption spectroscopy were prepared in the same way as those for the corresponding SERS spectra and were recorded in a Helios λ spectrometer. The colloidal suspensions were diluted to 10% in water and placed in 1 cm optical path quartz cuvette.

RESULTS AND DISCUSSION

VGD Adsorbed on AgNPs. The adsorption of VGD on AgNPs can be monitored through three different groups of key structural bands in the SERS spectrum: the bands appearing in the 1650−1550 cm^{-1} region, assigned to the C=C and C=N stretching modes, the ν(Ag−Cl) band in the low wavenumber region and the ν(C−C) inter-ring band positioned around 1300 cm^{-1}. The first two groups of bands inform about the interaction of the VGD with the metal, while the latter provides information regarding the dihedrical angle between the pyridine rings.[24]

(13) Otto, A. *J. Raman Spectrosc.* **2006**, *37*, 937–947.
(14) Le Ru, E. C.; Etchegoin, P. G.; Meyer, M. *J. Chem. Phys.* **2006**, *125*.
(15) Nie, S. M.; Emery, S. R. *Science* **1997**, *275*, 1102–1106.
(16) Guerrini, L.; Garcia-Ramos, J. V.; Domingo, C.; Sanchez-Cortes, S. *J. Phys. Chem. C* **2008**, *112*, 7527–7530.
(17) Vlckova, B.; Moskovits, M.; Pavel, I.; Siskova, K.; Sladkova, M.; Slouf, M. *Chem. Phys. Lett.* **2008**, *455*, 131–134.
(18) Monk, P. M. S. *The Viologens: Physicochemical Properties, Synthesis and Applications of the Salts of 4,4′-Bipyridine*; John Wiley and Sons: Chichester, U.K., 1998.
(19) Sun, Y.; Mayers, B. T.; Xia, Y. *Nano Lett.* **2002**, *2*, 481.
(20) Lee, P. C.; Meisel, D. *J. Phys. Chem.* **1982**, *86*, 3391–3395.
(21) Sanchez-Cortes, S.; Garcia-Ramos, J. V.; Morcillo, G.; Tinti, A. *J. Colloid Interface Sci.* **1995**, *175*, 358−368.
(22) Sanchez-Cortes, S.; Garcia-Ramos, J. V.; Morcillo, G. *J. Colloid Interface Sci.* **1994**, *167*, 428–436.
(23) Sanchez-Cortes, S.; Garcia-Ramos, J. V. *Surf. Sci.* **2001**, *473*, 133–142.
(24) Millan, J. I.; Garcia-Ramos, J. V.; Sanchez-Cortes, S. *J. Electroanal. Chem.* **2003**, *556*, 83–92.

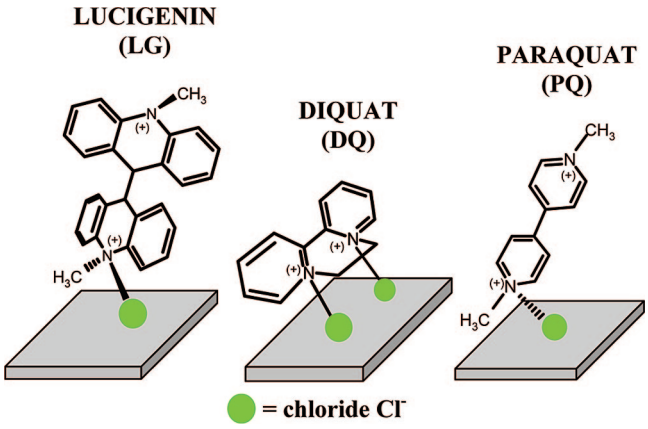

Figure 1. Outline of the proposed adsorption mechanisms and preferred orientations of LG, DQ, and PQ on the Ag surface.

A detailed analysis of the VGD adsorption was accomplished in previous works.[24,25] Briefly, we can report that LG is the VGD molecule showing the largest ability to form CT complexes with anions, since the specific spectral profile of the 1650−1500 cm^{-1} bands and the ν(Ag−Cl) feature observed on AgNPs were already seen in solution, where LG interacts with the counterions.[24] DQ is only able to form a CT complex with the adsorbed chloride on AgNPs, since no changes of marker bands were otherwise noted.[25] Finally, PQ does not show a tendency to form CT complexes even when binding the chloride anions adsorbed on the metal surface. Figure 1 illustrates the interacting schemes emerged from the SERS data (Figure S1; see the Supporting Information).

The adsorption of VGD induces clear changes in the architecture of Ag NPs in suspension, as can be demonstrated by the extinction spectra of the colloid. Although the larger aggregates likely provide the main contribution to the SERS signal, the effect of VGD on the NPs aggregation can be evaluated by studying the formation of dimers, which constitutes the previous step before the arrangement into multimers.

The VGD-driven formation of HS was monitored by following the plasmon band appearing in the 500−600 nm region, assigned to longitudinal plasmon in dimers.[16] LG turned out to be the best species to form junctions between NPs leading to appropriate HS for the detection of PYR.[16] In a previous work we have demonstrated the relationship between the appearance of the above plasmon absorption band and the formation of interparticle spaces, since the intensity of this band depends on the linker concentration.[16]

SERS and Plasmon Resonance Characterization of VGD/PYR Complexes. *SERS Spectra.* In the absence of VGD (Figure 2a), no SERS spectrum was obtained from PYR. The highly apolar nature of PYR prevents the necessary approach to the highly polar metal surface. As a control experiment, we used 9-(methylaminomethyl)-anthracene (MAMA) as a possible host molecule. However, this compound was not able to provide any PYR signal (Figure S2, see the Supporting Information), indicating that the simple changing of the metal surface properties to a more hydrophobic behavior is not sufficient to obtain the approaching of the pollutant. Most probably the monolayer formed by MAMA on the metal surface is too compact to allow the presence of cavities with the size demanded for the PYR detection, similarly to what is illustrated for a self-assembled monolayer of aliphatic and aromatic thiols on gold−germanium substrates.[26]

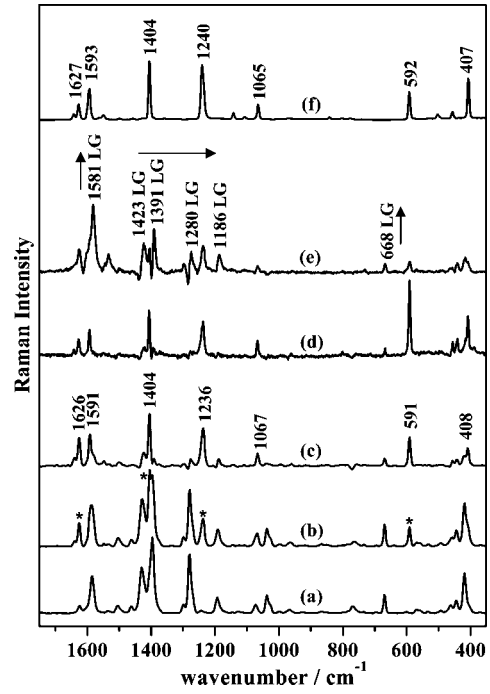

Figure 2. SERS spectra of (a) LG 10^{-6} M and (b) LG/PYR 10^{-6} M/10^{-6} M (the main PYR Raman bands are labeled with stars). Both spectra were recorded at λ_{exc} = 1064 nm. (c) SERS difference spectrum spectrum (b) − spectrum (a). (d and e) Same difference spectra but recorded at λ_{exc} = 785 nm and λ_{exc} = 514.5 nm, respectively. (f) Raman spectrum of PYR in the solid state at λ_{exc} = 1064 nm.

On the contrary, when the pollutant solution was added to the suspension of VGD functionalized NPs, intense PYR Raman bands can be seen because of the formation of the VGD/PYR complex (Figure 2b, for the case of LG). In addition, SERS spectra afford important structural information about the interaction mechanism of VGD and PAHs, as well as the strength of the Ag−(Cl^-)−VDG bridge, which can be also affected by the complexation of the pollutant. Moreover, the presence of the analyte can even modify the architecture of the VGD-NPs system, as pointed out by changes in the plasmon resonance spectrum. All these markers are summarized in Figure 3 and can be used to monitor the interaction of the analyte with the functionalized Ag NPs as shown below.

Figure 2 reports the SERS spectra obtained for LG and the LG/PYR complex at different excitation wavelengths (1064, 785, and 514.5 nm). As can be seen, changes in the main bands of PYR and LG are detected. The general enhancement of in-plane ring PYR bands indicates a preferably perpendicular orientation of the pollutant with respect to the metal surface as deduced from the SERS selection rules.[8] This is related to the formation of HS by LG, which ensure a perpendicular orientation of both the host and the pollutant. On the other hand, the enhancement of the bands at 590 and 1627 cm^{-1} suggests that the host−guest interaction mechanism is likely based on a $\pi-\pi$ stacking

(25) Lopez-Ramirez, M. R.; Guerrini, L.; Garcia-Ramos, J. V.; Sanchez-Cortes, S. *Vib. Spectrosc.* **2008**, *48*, 58–64.

(26) Domingo, C.; Garcia-Ramos, J. V.; Sanchez-Cortes, S.; Aznarez, J. A. *J. Mol. Struct.* **2003**, *661*, 419–427.

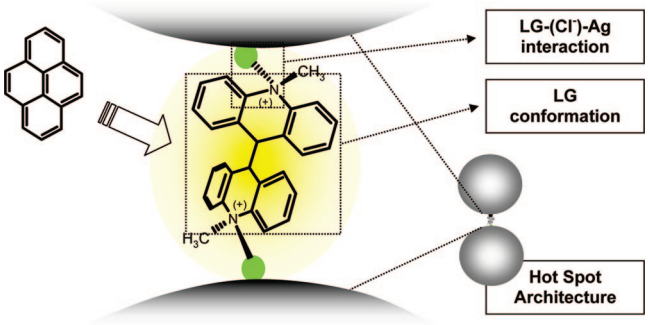

Figure 3. Schematic illustrating the effects of the PYR complexation on the LG-NPs sensing system.

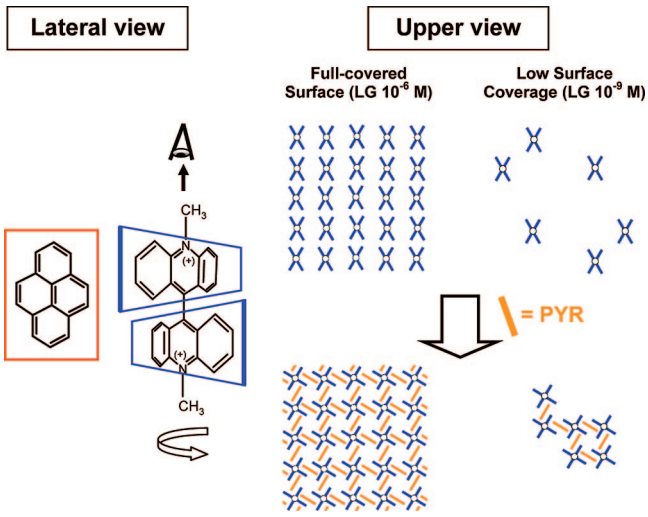

Figure 4. Schematic behavior of the acridine moieties of LG molecules adsorbed onto the metal surface once the interaction with PYR takes place.

interaction between the aromatic system of VGD and PYR, leading to a CT complex. The difference SERS spectrum (Figure 2e) reveals spectral changes related to the intensification of the LG−(Cl⁻)−Ag interaction. In fact, we observe an intensity increase of the ν(C═N) band at 1581 cm^{-1}, which is related to the formation of CT complexes, the downshifts of the LG bands at 1396 and 1430 cm^{-1}, assigned to ν(N$^+$−CH$_3$) motion, to 1391 and 1423 cm^{-1} respectively, and the intensity increase of the band at 668 cm^{-1}, assigned to the δ(CNC) vibration. Furthermore, the study of the sensing system at different excitation wavelengths allows a selective study of PYR or LG, as a decrease of the excitation wavelength induces the relative increase of the SERS intensity of LG with respect to the pollutant.

In addition, the group of bands sensitive to the inter-ring angle, appearing in the 1200−1300 cm^{-1} region, also undergoes remarkable spectral modifications. Specifically, a marked increase of the intensity and a shift downward of the aforementioned features are noticed, which may be related to a rotation of acridine rings toward lower coplanarity upon interaction with PYR. The downshift of the δ(C−H) vibration in acridine rings from 1193 to 1186 cm^{-1} (Figure 2e) is also related to the rotation around the main molecular axis as depicted in Figure 4. Thus, a strengthening of the LG−(Cl⁻)−Ag interaction and a subsequent rotation of the two

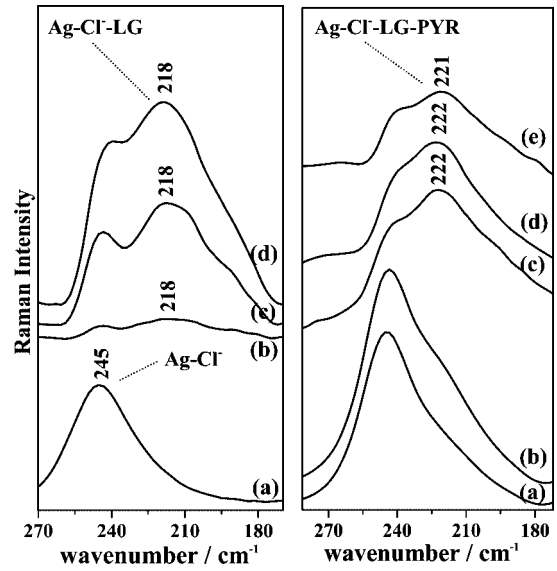

Figure 5. (Left panel) Effect of LG concentration on the ν(Ag−Cl) band in the FT-SERS spectra of LG. (a) SERS spectrum of Ag Citrate colloid aggregated by adding an aliquot of NaCl solution in the absence of LG. (b, c, and d) SERS difference spectra obtained upon subtraction of LG 10^{-8}M to LG 10^{-7}, 10^{-6}, and 10^{-5} M, respectively. (Right panel) Effect of the complex formation on the ν(Ag−Cl) band in the FT-SERS spectra of the LG/PYR complex. SERS spectra of (a) LG (10^{-6} M) and (b) LG/PYR (10^{-6} M/10^{-6} M). (d) Difference spectrum, spectrum (b) − spectrum (a). (c and e) Difference spectra of the LG/PYR (10^{-7} M/10^{-6} M) and (10^{-5} M/10^{-6} M), respectively.

acridine moieties of LG seem to occur as a consequence of the complexation with PYR.

The ν(Ag−Cl) band is also affected by the presence of PYR. The effect on this band is similar to what is observed by raising the LG concentration. Figure 5, left panel, displays the variation of the ν(Ag−Cl) band as a function of the LG concentration for a fixed halide concentration. In the absence of LG or at very low viologen concentrations, the ν(Ag−Cl) band appears at 245 cm^{-1} (Figure 5a, left panel). Upon an increase in the LG concentration, a feature at 220 cm^{-1} is seen, which can be attributed to the chloride ions linked simultaneously to Ag and LG leading to a ternary LG−(Cl⁻)−Ag interaction. The appearance of this new feature can be attributed to the weakening of the Ag−Cl bond upon the CT coordination of VGD with the halide.[25] At higher LG concentrations, a slight shift downward is also observed for the free Ag−Cl, probably due to a Stark effect, i.e., to the influence of the electric field of LG−(Cl⁻)−Ag groups formed besides the free Ag−Cl bonds. Figure 5, right panel, illustrates the variation of the ν(Ag−Cl) band in the presence of PYR at a fixed LG concentration. A new feature is seen at 220 cm^{-1}, suggesting that the number of LG−(Cl⁻)−Ag interactions also undergoes an increase in the presence of PYR.

At a very low LG concentration (10^{-9} M), a drastic enhancement of the SERS spectrum in the presence of PYR is observed (Figure 6). This fact demonstrates the positive effect of PYR in the increasing of LG−(Cl⁻)−Ag interactions on the surface. We suggest that the number of hot spots induced by LG is poor at low viologen concentration, due to the still high negative potential at the NPs surfaces and the higher dispersion of the LG molecules on the metal surface (Figure 4, right panel). Thus, the main part of LG molecules must be linked to the metal through

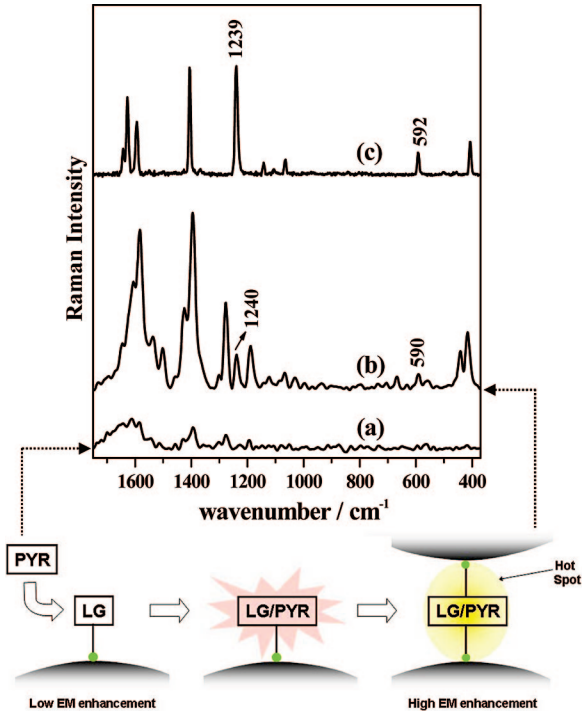

Figure 6. SERS spectra of (a) LG 10^{-9} M and (b) LG/PYR (10^{-9} M/10^{-6} M). (c) Raman spectrum of PYR in the solid state. All the spectra were recorded at $\lambda_{exc} = 514.5$ nm.

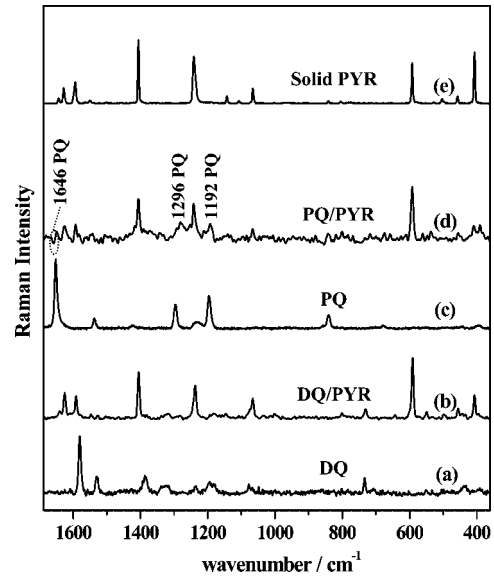

Figure 7. (a) SERS spectrum of DQ (10^{-4} M) and (b) SERS difference spectrum of DQ/PYR (10^{-5} M/10^{-6} M). (c) SERS spectrum of PQ (10^{-5} M) and (d) SERS difference spectrum of PQ/PYR (10^{-5} M/10^{-6} M). (e) Raman spectrum of the solid PYR. All the spectra were recorded at $\lambda_{exc} = 785$ nm.

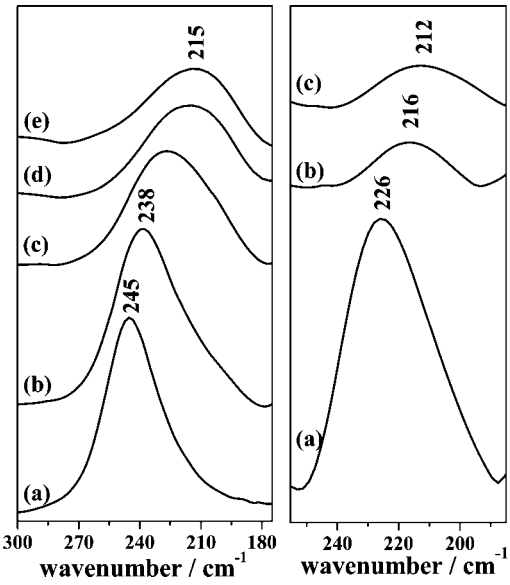

Figure 8. (Left panel) Effect of DQ concentration on the ν(Ag−Cl) band in the FT-SERS spectra of DQ. (a) SERS spectrum of Ag citrate colloid aggregated by adding an aliquot of NaCl solution in the absence of DQ. (b, c, d, and e) SERS difference spectra obtained upon subtraction of DQ 10^{-7} M from DQ 10^{-6}, 10^{-5}, 7×10^{-5}, and 10^{-4} M, respectively. (Right panel) Effect of the complex formation on the ν(Ag−Cl) band in the FT-SERS spectra of the DQ/PYR complex. (a, b, and c) SERS difference spectra of the DQ/PYR (10^{-7} M/10^{-6} M), (10^{-5} M/10^{-6} M), and (10^{-4} M/10^{-6} M), respectively.

one of the acridine sides (Figure 6). At these conditions, the NPs approaching is not favored. However, when the LG/PYR complexation takes place, we observe an increase of the viologen affinity toward the metal surface, resulting in an increase of interparticle junctions and a further SERS enhancement of the Raman signal of both LG and PYR in the complex. This phenomenon can be explained in terms of a cooperative effect of PYR complexation, which induces the formation of LG patches on the surface with enough strength as to allow the linking of two particles, as depicted in Figure 4, right panel. The detection of PYR at this very low host surface coverage further supports the preferable placement of the LG/PYR complex at the HS.

In the case of DQ, no significant changes in the SERS spectrum of the viologen were observed upon complexation with the pollutant (Figure 7b). As it was expected, the stiffness imposed on the geometry of the host molecule by the ethylene chain connecting the two pyridine rings avoids the rotation around the C−C inter-ring bond. Therefore DQ may be less prone to alter its adsorption geometry compared to LG, even when interacting with the PYR.

The presence of the ligand also affects the interaction between the DQ and the metal, as for LG. The effect of the PYR addition to the ν(Ag−Cl) band is shown in Figure 8, left panel.[25] In this case the amount of free Ag−Cl sites is lower due to the higher number of DQ−(Cl^-)−Ag interactions in relation to LG. This is likely due to the simultaneous interaction of both N atoms with the surface, as depicted in Figure 1. The complexation of the pollutant produces a shift downward of the ν(Ag−Cl) feature with the appearance of new bands at 226 cm^{-1} (at 10^{-6} M of DQ) and at 212 cm^{-1}, as the concentration of DQ is raised to 10^{-4} M (Figure 8, right panel). This can be related to the existence of two different types of DQ adsorbed on the metal surface instead of one as deduced for LG (Figure 3). In fact, we suggested the formation of two different adsorption arrangements involving two or three DQ molecules in a bridge between two NPs,[16] where the amount of the three-unit bridge growths with respect to the two-unit geometry by raising the DQ concentration.

Finally, the interaction of PYR with PQ seems to induce a rotation of the viologen pyridine rings around the C−C inter-ring bond toward lower coplanarity, as deduced from the downshifts

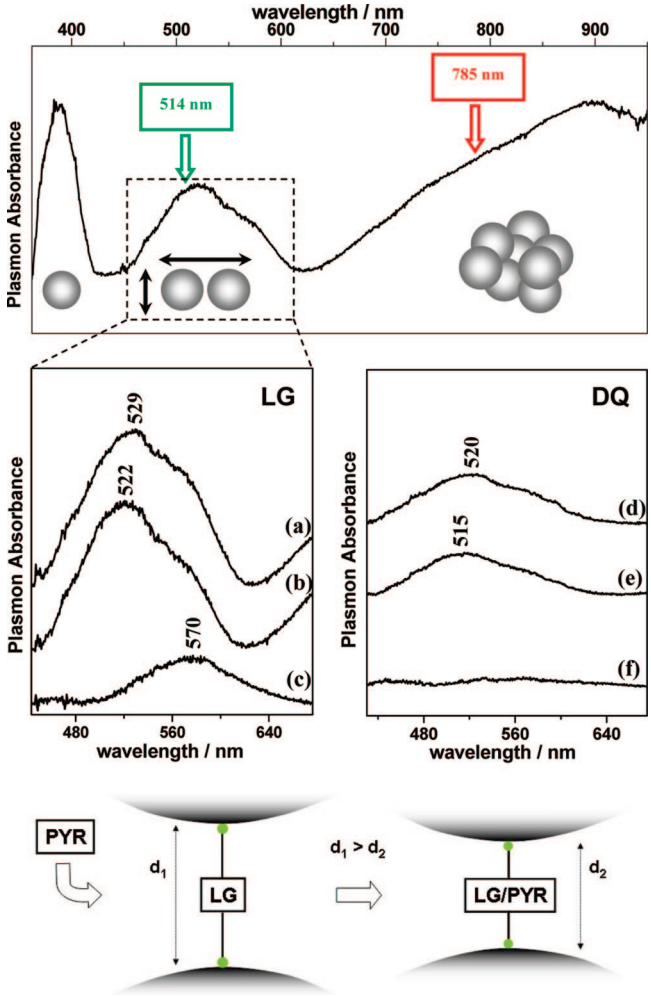

Figure 9. (Top) Difference absorption spectrum of Ag NPs aggregated in the presence of LG (10^{-6} M), obtained upon subtraction of the absorption spectrum of Ag NPs aggregated with only chloride anions, displaying plasmon absorptions corresponding to monomer or transversal plasmons in chains (383 nm), longitudinal plasmons in dimers (500−600 nm), and multimers (broadband increasing above 700 nm). (Middle) Plasmon absorbance bands observed in the 500−600 nm region assigned to Ag NPs dimers obtained upon aggregation with (left panel) (a) LG/PYR (10^{-6} M/10^{-6} M) and (b) LG (10^{-6} M). (c) Difference spectra spectrum (a) − spectrum (b). Right panel (d) DQ/PYR (10^{-4} M/10^{-6} M) and (e) DQ (10^{-4} M). (f) Difference spectra spectrum (d) − spectrum (e). (Bottom) Schematic illustrating the decrease of interparticle distance after the formation of the LG/PYR complex.

of the PQ bands at 1646, 1296, and 1196 cm^{-1} (Figure 7d). However, no spectral changes were detected in the ν(Ag−Cl) band upon addition of PYR. This is indeed related to the weaker interaction of PQ with the Ag−Cl sites on the surface.

Plasmon Absorption Spectra. The effect of PYR on VGD-NPs systems can be also noted on the aggregation pattern and the architecture of the resulting NPs aggregates, as followed by their plasmon absorption spectra.

First of all, the effect of VGD on the AgNPs aggregates architecture is revealed when subtracting the plasmon resonance spectrum of the colloid in the presence of chloride from the spectrum of the same sample but after the addition of the viologen (Figure 9, top panel, in the case of LG). The resulting difference spectrum shows a band in the 500−600 nm region, which can be attributed to the dimers created by the bifunctional linker.[16]

Figure 9, middle panels, illustrates the effects of the PYR complexation on the dimer band in the case of LG/PYR and DQ/PYR complexes. Regarding the LG-NPs system, a new feature is observed at 570 nm (Figure 9c, middle left panel), indicating that the CT interaction with the pollutant leads to a higher coupling between the NPs, i.e., reduction of the interparticle distance by the tightening of the NP−(Cl^-)−LG−(Cl^-)−NP bridging bonds, as outlined in Figure 9, bottom scheme. Indeed, this is related to the changes of the host conformation highlighted by the SERS spectra above. The broadness of this new contribution may be explained again in terms of flexibility of the host molecule, considering that the LG molecule is able to rotate around the interring C−C bond to different extents, adopting several slightly distinct configurations. Moreover, the dimer band area increases ~15% in the presence of PYR. This agrees with the increasing of the HS formation efficiency originating from the LG−PYR interaction, as deduced before (Figure 6).

On the contrary, as well as the SERS spectrum of DQ, the complexation with the pollutant does not affect the dimer band of DQ-NPs (Figure 9f, middle right panel). This agrees with the negligible conformation change deduced for DQ in the presence of PYR.

In the case of PQ-NPs, no plasmon band in the 500−600 nm region was observed, suggesting that PQ is a poor or void HS inducer. Therefore, the PYR detection achieved by PQ-NPs is fairly due only to the successful functionalization of the metal surface whereas lacks the additional EM enhancement provided by the HS formation. As a result, PQ can be used as a control molecule to test the ability of other bifunctional linkers, such as LG and DQ, in the formation of interparticle junctions.

Optimization of PAHs Detection at Different VGD Concentrations. The entire architecture of the self-assembled VGD on the metal surface, as well as their conformations, and the number of active sites available for the complexation with the pollutant are key factors determining the final host ability of the sensing system. Consequently, a complete study of the PYR detection at different surface coverage was performed by monitoring the SERS intensity of the PYR band at 590 cm^{-1} in a wide range of VGD concentrations (Figure 10, left panel). The study was performed at three excitation laser wavelengths and keeping a constant PYR concentration of 10^{-6} M. The feature at 590 cm^{-1} was selected as the marker band because it appears in a spectral region rather free of VGD bands and is one of the strongest bands in the PYR spectrum.

In general, LG-NPs shows the best results for all excitation wavelengths investigated showing the highest detection ability in a wider range of surface covering. In contrast, PQ-NP displays the lowest effectiveness for all the excitation at all the studied host concentrations. This agrees with the lower activity of PQ to induce the formation of interparticle junctions. Finally, DQ-NPs provided intense PYR signal only at concentrations bigger than 10^{-6} M, reaching a maximum at 10^{-4} M, specifically when the three-unit junctions are formed to a greater extent.[16]

Two main factors can affect the host ability of the adsorbed VGDs: the chemical affinity toward the analyte and the geometrical properties of the intercavities provided by the self-assembled host

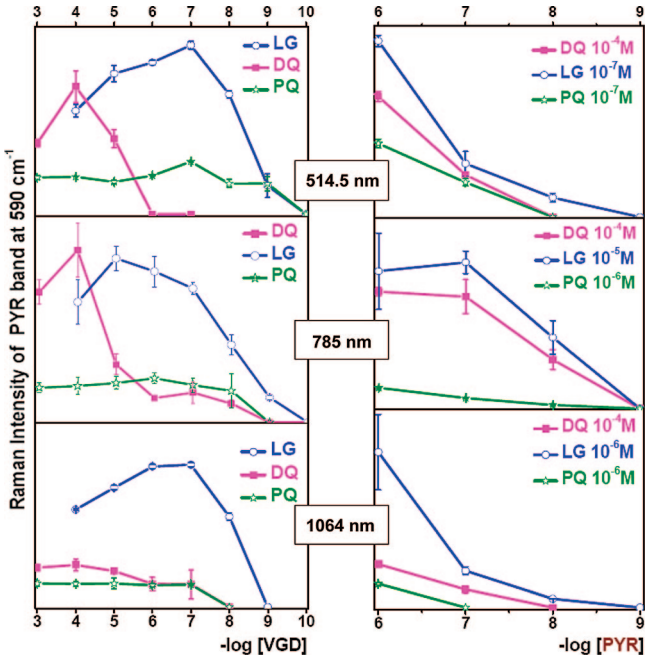

Figure 10. (Left panel) Raman intensity of the 590 cm^{-1} marker band of PYR against the VGD concentration at different excitation wavelengths. From the top to the bottom, λ_{exc} = 514.5 nm, λ_{exc} = 785 nm, and λ_{exc} = 1064 nm. (Right panel) Raman intensity of the 590 cm^{-1} marker band of PYR against the PYR concentration at different excitation wavelengths. From the top to the bottom, λ_{exc} = 514.5 nm, λ_{exc} = 785 nm, and λ_{exc} = 1064 nm. The VGD concentrations are constants. All the measurements were carried out on Ag colloid suspension (macrosetup).

molecules. The aromatic extension of VGD plays an important role in the affinity toward the aromatic PAHs. In this sense, LG and the whole three-unit DQ bridge provide the best hosting characteristic to allocate PYR. On the contrary, the lower aromatic size of PQ reduces its affinity in relation to these analytes. This affinity is further reduced by taking into account that a weaker interaction was deduced for the PQ−(Cl^-)−Ag bridge. Besides, we suggest that the intermolecular cavities provided by the PQ molecules and the DQ molecules organized in the two-unit bridge are smaller and then less suitable for the PYR placement compared to those provided by the rotating acridine moieties of LG and the three-unit junctions of DQ.

It is particularly interesting to investigate the effect of the excitation wavelength on the sensing effectiveness of the VGD-NPs systems, as the laser at 514.5 nm will predominantly excite the dimers while the lines at 785 and 1064 nm excite the multimers (Figure 9, top panel). This dependence from the excitation wavelength is notably marked for the DQ-NPs system. In fact, at 514.5 nm, DQ-NPs are only active in the detection of PYR at concentrations higher than 10^{-6} M, i.e., when the dimers are largely formed by three-unit DQ bridges, the most active interaction geometries for the detection of PYR. However, the detection ability of DQ-NPs decreases significantly when using the line at 1064 nm. This is likely due to the formation of globular aggregates which exhibit a plasmon resonance band below 1064 nm. In contrast, the detection ability of LG-NPs practically did not change on varying the excitation wavelength, always exhibiting the maximum performances in the 10^{-5}−10^{-7} M concentration range. The high detection ability shown at

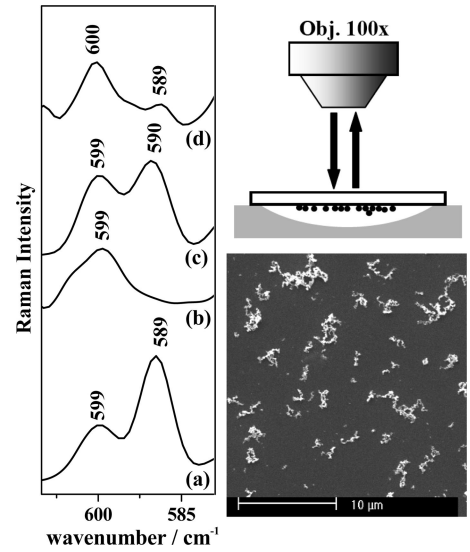

Figure 11. (Left panel) (a) Macro SERS spectra of LG/PYR (10^{-6}/10^{-8}M). Micro SERS spectra of (b) LG 10^{-6}M, (c) LG/PYR (10^{-6}/5 × 10^{-8}M), and (d) LG/PYR (10^{-6}/5 × 10^{-10}M). All the Micro-SERS have been obtained averaging five different spectrum recorded at five different points over the NP aggregate selected. All the spectra were recorded at λ_{exc} = 785 nm. (Right panel) Top: micro-SERS setup. Bottom: SEM micrograph of the dried colloid.

1064 nm by LG-NPs is possibly related to the formation of more linear aggregates, which support plasmon resonances toward the near IR region.

Limit of Detection. Once the optimum VGD concentrations providing the higher pollutant SERS intensities for each excitation wavelengths were identified, we kept them constant and studies of the limit of detections were performed (Figure 10, right panel, all the measurements were carried out on Ag colloid suspension). Once more, LG-NPs gave the best results, allowing the detection of the PYR marker band down to nanomoles.

Micro-SERS measurements were performed by immobilizing the colloidal NPs previously functionalized with LG 10^{-6} M on a glass. Aliquots of the PYR solutions at different concentrations were then put in contact with the dried colloid and analyzed. Figure 11 displays the details of the micro-SERS spectra in the 610−580 cm^{-1} spectral range. The SERS of LG was first acquired in the absence of PYR (Figure 11b), then in the presence of the pollutant at different concentrations, from 10^{-8} M (Figure 11c) down to 5 × 10^{-9} M (Figure 11d). The latter value was the lowest concentration which provided a detectable PYR marker band. All the microspectra presented were obtained by averaging five different acquisitions on five different locations of the selected NPs aggregate. Considering the surface lighted equal to 1 μm^2 and a homogeneous distribution of PYR molecules over the sample, we estimated the number of PYR molecules detected around 80, which corresponds to about 0.13 zmol. This LOD is much lower than those reported elsewhere in the analysis of PAHs in a water solution.[27−30] The LODs were calculated considering the lowest PYR concentration leading to a

(27) Bourdat-Deschamps, M.; Daudin, J. J.; Barriuso, E. *J. Chromatogr., A* **2007**, *1167*, 143–153.
(28) Zuazagoitia, D.; Millan, E.; Garcia, R. *Chromatographia* **2007**, *66*, 773–777.
(29) Cai, Z. Q.; Zhu, Y. X.; Zhang, Y. *Spectrochim. Acta, Part A: Mol. Biomol. Spectrosc.* **2008**, *69*, 130–133.

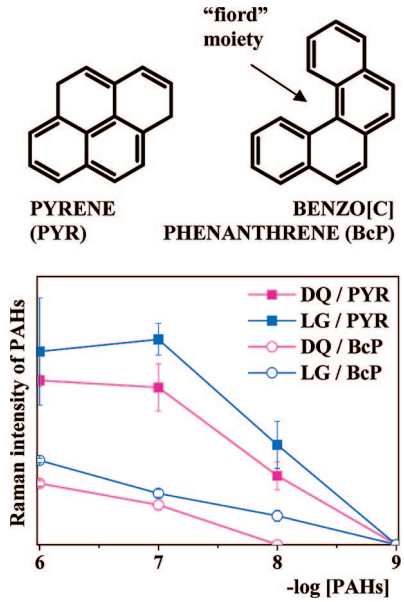

Figure 12. Raman intensities of the PYR marker band at 590 cm^{-1} and the BcP marker band at 1380 cm^{-1} against the PAHs concentration. The LG and DQ concentrations were kept constant at 10^{-4} and 10^{-6} M, respectively. The detection limit study was carried out at λ_{exc} = 785 nm in macroconditions. Top: molecular structures of pyrene (PYR) and benzo[*c*]phenanthrene (BcP).

SERS intensity of the marker band at 590 cm^{-1} which produces a signal/noise ratio > 2.

In Figure 12, the LODs of PYR and BcP are compared. The DQ and LG concentrations were kept constants at 10^{-4} and 10^{-5} M, respectively, and the laser line at 785 nm was employed as the excitation source. As can be seen, the efficiencies of both DQ- and LG-NPs sensing systems on the detection of BcP are lower than in the case of PYR. By contrast, the SERS sensing platform based on the self-assembling of dithiocarbamate calix[4]arene (DTCX) on Ag NPs[11] presented a higher host ability for BcP than for PYR. This opposite result may be possibly due to the different properties of the host cavities provided by the aforementioned functionalizations. Most probably, the higher affinity of BcP to bind DTCX is associated with the existence of a "fiord" moiety in this molecule (Figure 12) which makes the BcP structure twisted from planarity[18] and, thus, more suitable for the positioning inside the "cuplike" shape cavity of the calixarene derivative. Conversely, the fully planar acridine portions of the LG and the largely planar bipyridine backbone of DQ may lead to a stronger interaction with the fully planar PYR molecule. The LG-NPs system was also successfully employed in the detection of aliphatic pesticides,[31] although the LOD exhibited is much lower than that displayed in the analysis of PAHs.

CONCLUSIONS

SERS nanosensors can be prepared by using Ag NPs functionalized with viologens, which can be used for the specific detection of PAHs. In particular, LG and DQ interact strongly with the metal surface via VGD−(Cl^-)−Ag bridges and demonstrated their good capabilities in the of PYR and BcP by means of intermolecular cavities with high affinity toward the analytes. Besides, they are able to create interparticle junctions or HS where a huge EM enhancement is localized. In contrast, PQ showed a poorer ability in the PYR detection, due to the different adsorption of this viologen on Ag, which accounts for a lower formation of HS.

Specifically, the functionalization with LG provided the most powerful and stable VGD-NPs nanosensor, due to its bifunctional nature and its large aromatic character. In fact, we reported the SERS detection of PYR down to the nanomole range in macroconditions and in the zeptomole range from spectra obtained by single NPs aggregates (micro setup). Besides, the detection performance of LG-NPs is further intensified by a cooperative effect of the analyte, since PYR is able to favor the formation of a higher number of intermolecular cavities and, in turn, of interparticle HS. Conversely, the DQ-NPs system presented a high detection ability limited to relatively high viologen concentrations and for laser excitation wavelengths falling in the visible region.

SERS spectra afford important structural information about the interaction mechanism of VGD and PAHs, revealing the formation of a CT complex between the VGD and PYR and changes in the host conformation. In addition, other special features such as the position of the ν(Ag−Cl) band and the plasmon resonance contribution assigned to Ag dimers are important to evaluate the sensing ability of VGD-NPs systems.

The results of this work point out a new strategy to be applied in the ultratrace SERS detection of molecules with low affinity toward the metal surface. We suggest that the functionalization of the metal surface has to be performed by using a host species possessing at least four main features: (i) high affinity toward the NPs surface, (ii) high affinity toward the target molecule, (iii) ability to provide proper cavities where the analyte can be located, and (iv) bifunctionality, in order to induce HS formation and therefore the approaching of the target molecule near to these area where the EM intensification is enormous. This work demonstrated the usefulness of both SERS and nanoparticle plasmon resonance in the detection of pollutants.

ACKNOWLEDGMENT

Authors acknowledge Dirección General de Investigación (Ministerio de Educación y Ciencia) Project Number FIS2007-63065 and Comunidad Autónoma de Madrid Project Number S-0505/TIC/0191 MICROSERES for financial support. L.G. acknowledges CSIC for an I3P fellowship.

SUPPORTING INFORMATION AVAILABLE

Additional information as noted in text. This material is available free of charge via the Internet at http://pubs.acs.org.

Received for review October 14, 2008. Accepted December 26, 2008.

AC8021746

(30) de Sousa, J. R.; Parente, M. M. V.; Diogenes, L. C. N.; Lopes, L. G. F.; Neto, P. D.; Temperini, M. L. A.; Batista, A. A.; Moreira, I. D. *J. Electroanal. Chem.* **2004**, *566*, 443–449.

(31) Guerrini, L.; Aliaga, A. E.; Carcamo, J.; Gomez-Jeria, J. S.; Sanchez-Cortes, S.; Campos-Vallette, M. M.; Garcia-Ramos, J. V. *Anal. Chim. Acta* **2008**, *624*, 286–293.